Synergy of turbulent momentum drive and magnetic braking

R Varennes, X Garbet, L Vermare, Y Sarazin, Guilhem Dif-Pradalier, V Grandgirard, P Ghendrih, P Donnel, M Peret, K Obrejan, et al.

Synergy of turbulent momentum drive and magnetic braking

R. Varennes[1], X. Garbet[1], L. Vermare[2], Y. Sarazin[1], G. Dif-Pradalier[1], V. Grandgirard[1], P. Ghendrih[1], P. Donnel[1], M. Peret[1], K. Obrejan[1], E. Bourne[1]
[1] *CEA, IRFM, F-13108 Saint-Paul-Lez-Durance, France.*
[2] *LPP, CNRS, Ecole polytechnique, 91128 Palaiseau, France.*

In absence of external torque, plasma rotation in tokamaks results from a synergy between collisional magnetic braking and turbulent drive. The outcome of this competition/cooperation is essential to determine the plasma flow. A reduced model, supported by gyrokinetic simulations, is first used to explain and quantify the competition only. The ripple amplitude above which magnetic drag overcomes turbulent viscosity is obtained. The synergetic impact of ripple on the turbulent toroidal Reynolds stress is explored. Simulations show that the main effect comes from an enhancement of the radial electric field shear by the ripple, which in turn impacts the residual stress.

Mean flows and especially toroidal rotation play a key role in confinement properties of tokamak plasmas. Indeed, numerous experiments have highlighted the link between plasma rotation and improved plasma performance [1–5]. On most medium size tokamaks, rotation is controllable using the external torque exerted by tangential neutral beam injection. However in reactor-size tokamaks, including ITER, external torque is expected to be small [6], so that the plasma rotation will likely be driven by intrinsic plasma mechanisms. Intrinsic generation of rotation results from symmetry breaking [7]. Therefore, toroidal asymmetry of the magnetic field plays a leading role in rotation drive, as realistic magnetic configurations always include non-axisymmetric perturbations. They result from error fields due to coil misalignment, magnetohydrodynamic instabilities, externally applied perturbations or magnetic field modulations due to the finite number of toroidal coils, called *ripple*. This paper focuses on the latter. Toroidal magnetic ripple constrains the toroidal torque through magnetic braking, i.e. the force resulting from the magnetic field inhomogeneity on particle magnetic moments. This force substantially changes the plasma rotation even for small amplitude perturbations [8]. The resulting torque, called *Neoclassical Toroidal Viscosity*, and its impact on toroidal rotation have been experimentally observed [9–13] and widely studied theoretically [14–25] as well as numerically [26–30]. The other main symmetry breaking mechanism is turbulence in presence of a background $E \times B$ shear, which has also been extensively studied [7, 31–43]. Yet, the possible competing and/or synergetic effects of extrinsic (ripple) versus self-generated (turbulence) asymmetries on rotation has drawn little [44] attention so far. Consequences are of prime importance, since any modification of mean flows impacts the radial electric field, and therefore also the transition toward improved confinement regimes [45]. In this paper, the ripple amplitude threshold δ_c below which turbulence governs plasma flows is estimated theoretically, first without any cross-talk between ripple and turbulence. It is in agreement with nonlinear gyrokinetic simulations using the GYSELA code [46] and given with a simple expression. Secondly, the interplay between turbulence and ripple regarding the toroidal velocity is studied thanks to comprehensive gyrokinetic simulations for the first time. The modification of the spectral intensity by ripple through mode-coupling is found negligible. However, ripple is found to modify the toroidal Reynolds stress through the radial electric field shear.

The ripple and turbulent contributions to the toroidal velocity V_T appear in the toroidal momentum conservation expressed within toroidal coordinates (r, θ, φ):

$$\partial_t V_T = \mathcal{M} - r^{-1}(r\Pi)' \tag{1}$$

Where a prime stands for the radial derivation, $\mathcal{M}$ is the magnetic braking and Π is the turbulent radial flux of toroidal momentum, called toroidal Reynolds stress. Each contribution deserves some attention. The magnetic braking is derived within neoclassical theory, i.e. a kinetic derivation describing the resonant enhancement of collisional transport processes. A well established result of this theory in axisymmetric configurations is the degeneracy between the toroidal velocity V_T and the radial electric field E_r. Ripple breaks axisymmetry, leading to non-ambipolar diffusion of particles and heat [14]. The resulting radial electric field constrains the toroidal torque through magnetic braking $\mathcal{M}$, removing the degeneracy. The magnetic braking is defined as the following fluid moment of the ion distribution function F:

$$\mathcal{M} = \frac{-1}{nm}\left\langle \int d^3\boldsymbol{v} R\boldsymbol{\nabla}\varphi \cdot \boldsymbol{\nabla}(\mu\tilde{B})F \right\rangle \tag{2}$$

Where $\langle . \rangle$ denotes a flux surface average, μ the magnetic moment, m the particle mass, n the density and R the tokamak major radius. The toroidal perturbation of the magnetic field amplitude due to ripple reads $\tilde{B} = B(r,\theta)\delta(r,\theta)\cos(N_c\varphi)$, where B is the axisymmetric magnetic field amplitude, δ the ripple amplitude and N_c the number of toroidal coils. $\mathcal{M}$ is thus the force due to toroidal asymmetry of the magnetic field. It takes the

form of a friction [14]:

$$\mathcal{M} = -\nu_\varphi \left(V_T - V_{neo}\right) \tag{3}$$

Where V_{neo} is the target velocity fixed by collisional processes and ν_φ is the magnetic drag coefficient. The former, roughly independent of δ, is in the counter direction as the non-ambipolar particle flux results in a negative E_r [22, 24]. Both V_{neo} and ν_φ are predicted by neoclassical theory. Dedicated simulations including ripple perturbation have found that GYSELA results are consistent with these theoretical predictions. Ripple perturbation implementation in GYSELA is detailed in the Supplemental Material [47]. In the absence of turbulence, V_T dynamic is then governed by the magnetic drag coefficient ν_φ which depends on the ripple amplitude δ. The other drive mechanism is turbulence through the toroidal Reynolds stress Π. Keeping only turbulent contributions, the toroidal component of the stress tensor takes the form [32, 33, 35]:

$$\Pi = -\chi V_T' + \mathcal{V} V_T + \Pi_{res} \tag{4}$$

Where χ is a turbulent viscosity coefficient, $\mathcal{V}$ a pinch coefficient and Π_{res} the residual stress. The latter describes the momentum exchange between waves and particles, which acts as the only source of intrinsic plasma rotation in the axisymmetric case. Combining those mechanisms, the equilibrium toroidal velocity V_{Teq} reads:

$$V_{Teq} = \frac{\nu_\varphi V_{neo} - r^{-1}(r\Pi_{res})'}{\nu_\varphi + \chi\lambda_v + \mathcal{V}\kappa_v} \tag{5}$$

With $\lambda_v = -(r\chi V_{Teq}')'/(r\chi V_{Teq})$ and $\kappa_v = (r\mathcal{V}V_{Teq})'/(r\mathcal{V}V_{Teq})$. As discussed below, this equation allows one to estimate the ripple amplitude for which magnetic braking overcomes turbulence. Note that any interplay between ripple and turbulence is not considered here, but will be discussed later. Since ν_φ is an increasing monotonic function of the ripple amplitude δ then at low ripple, $\delta \to 0$, neoclassical terms vanish so $V_{Teq} \to V_{turb} = -\frac{r^{-1}(r\Pi_{res})'}{\chi\lambda_v + \mathcal{V}\kappa_v}$. At high ripple, $\delta \to \infty$, turbulent terms become negligible so $V_{Teq} \to V_{neo}$. Computing the radial profile of V_{Teq} as a function of the ripple amplitude requires solving a transport equation. However a "critical ripple" amplitude δ_c can be devised such that magnetic braking is dominant when $\delta > \delta_c$. As shown Fig.1, this critical value can be roughly defined as $V_{Teq}(\delta_c) = (V_{neo} + V_{turb})/2$ leading to $\nu_\varphi(\delta_c) = |\chi\lambda_v + \mathcal{V}\kappa_v|$. As already mentioned, predictions on ν_φ and its dependence on δ are known. Conversely, there are so far no reliable analytical prediction about χ and $\mathcal{V}$. Determining those coefficients is actually an active topic of both experimental and theoretical research. Here they are determined with four gyrokinetic simulations of ITG turbulence, performed with adiabatic

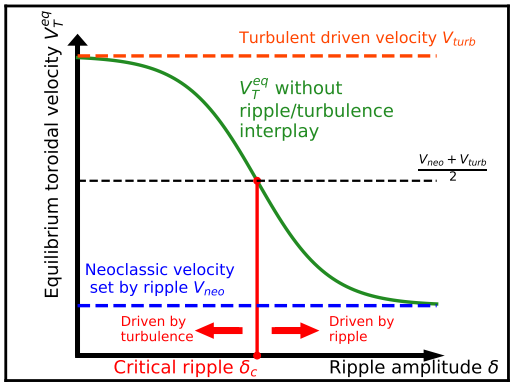

FIG. 1. Sketch of the modelled ripple/turbulence competition on the equilibrium toroidal velocity estimated with local momentum conservation in case of co-current V_{turb}. The synergistic effects are not accounted for here, but are detailed further below.

electrons, of a typical Tore Supra discharge [48] without ripple (i.e. $\delta = 0$). Details on simulations parameters can be found in the Supplemental Material [47]. Taking advantage of the Π structure Eq.4, one can determine χ and $\mathcal{V}$ for each radius by initializing the simulations with different toroidal velocity. A least square method using the resulting V_T, V_T' and Π profiles after saturation of turbulence, displayed on Fig.2, gives access to these coefficients. As indicated by the clear correlation between Reynolds stress and toroidal velocity shear, the viscosity term is dominant. The resulting turbulent viscous contribution to V_{Teq} is displayed in Fig.3 (orange lines). In addition, at $r/a \approx 0.5$ with a the minor radius, where V_T' vanishes and V_T is extremal, Π reaches the same value for each simulation. Therefore the pinch term is negligible, as expected for adiabatic electrons [7], so that Π is dominated by the residual stress at vanishing V_T'. Notice that, even when kinetic electrons are accounted for, the pinch contribution is expected to be subdominant compared with the viscous one, as observed experimentally. From now on, the critical ripple expression then becomes $\nu_\varphi(\delta_c) \approx \chi|\lambda_v|$. To check the relevance of the prediction regarding δ_c, two additional simulations with finite ripple, and consequently finite magnetic drag, such that $\nu_\varphi \ll \chi|\lambda_v|$ and $\nu_\varphi \gg \chi|\lambda_v|$ were run, cf. Fig.3 (blue lines). Since the physics of the boundary acts as a complex momentum sink, controlled by orbit losses, momentum flux carried by waves [31] and scrape-off layer interactions, a model ripple amplitude is chosen with a radially Gaussian envelope centered at mid-radius: $\delta(r) = \delta_0 \exp\left(-4(r/a - 0.5)^2\right)$. This ensures the disentanglement between boundary conditions and intrinsic physics in a controlled way. In those simulations the mid-radius ripple amplitudes are $\delta_0 = 0.1\%$ and $\delta_0 = 1\%$. The time evolution of the toroidal velocity V_T – respectively of the radial

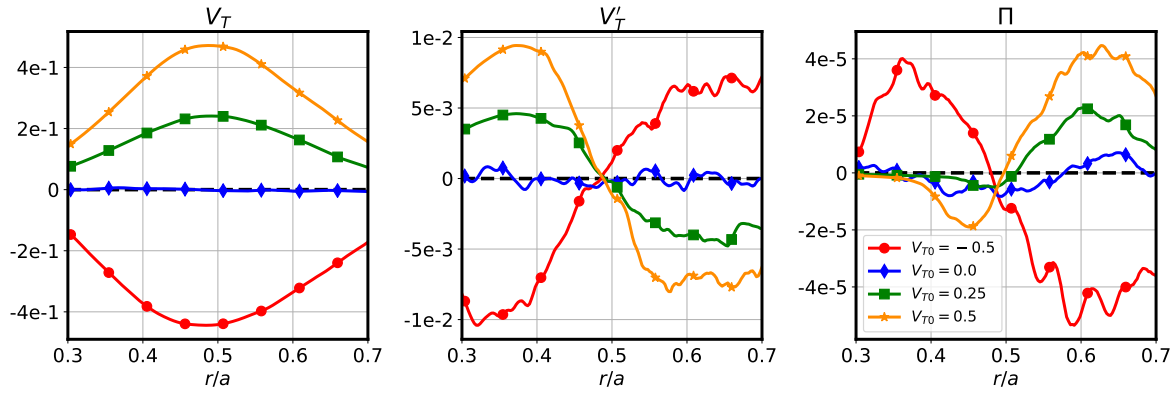

FIG. 2. Radial profiles of the stress tensor Π, toroidal velocity V_T and its shear V'_T taken at turbulent saturation for simulations without ripple and with different initial toroidal velocity profiles $V_T(t=0) = V_{T0}\exp\left(-4(r/a-0.5)^2\right)$ with a the minor radius. Velocities are normalised to the ion thermal velocity and lengths to ion Larmor radius ρ_i.

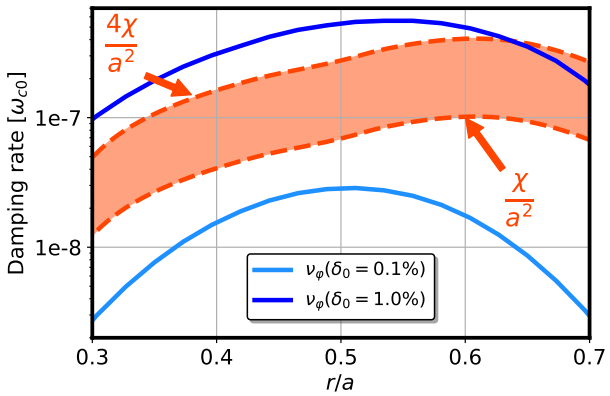

FIG. 3. Radial profile of magnetic drag ν_φ for different ripple amplitudes and the turbulent viscous contribution $\chi\lambda_v$. Orange zone represents $\chi|\lambda_v|$ for $a/2 \leq |\lambda_v|^{-1/2} \leq a$. Time is normalized to the cyclotron period ω_{c0}^{-1}.

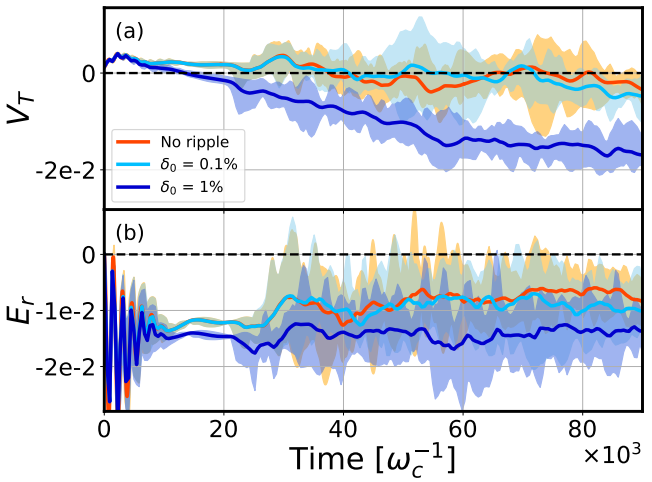

FIG. 4. Time trace of the toroidal velocity V_T (a) and the radial electric field E_r (b) in $0.45 < r/a < 0.55$ (shaded areas, mean: solid lines) for different ripple amplitudes.

electric field E_r – for each case near mid-radius is shown on Fig.4a – respectively Fig.4b. The $\delta_0 = 0.1\%$ case exhibits no significant difference with the axisymmetric case $\delta_0 = 0$, neither regarding V_T nor E_r. Conversely, the toroidal velocity in the $\delta_0 = 1\%$ case, deeply in the counter-current direction, is driven by magnetic braking. Also, E_r increases roughly by a factor 1.5. The critical ripple amplitude then stands out as a practical landmark to determine the main driving flow mechanism. A rule of thumb is proposed here to evaluate the order of magnitude of δ_c. First, one can approximate the magnetic drag to its asymptotic value in the so-called *ripple-plateau* regime of collisionality. In most tokamaks, including ITER, this regime is the most relevant and states that $\nu_\varphi \sim \frac{N_c V_{th}}{R}\delta^2$ where V_{th} is the ion thermal velocity. For the turbulent viscosity, one can consider the gyroBohm scaling $\chi \sim \frac{\rho_i^2 V_{th}}{L_T}$ where L_T is the temperature gradient length and ρ_i the ion Larmor radius. The validity of those approximations was verified with GYSELA simulations and is detailed in the Supplemental Material [47]. Under these hypotheses, the critical ripple amplitude can be estimated as $\delta_c \sim \rho_\star \varepsilon \left(\frac{1}{N_c}\frac{R}{L_T}R^2|\lambda_v|\right)^{1/2}$ where ε is the inverse aspect ratio and $\rho_\star = \rho_i/a$. A naive application on a Tore Supra ohmic discharge at $r/a = 0.8$ with $\rho_\star^{-1} = 700$, $R/L_T = 12$, $N_C = 18$ and $|\lambda_v|^{-1/2} \sim 20cm$ [49] gives $\delta_c \approx 0.4\%$ which is way lower than the actual ripple amplitude in Tore Supra at this location. Consistently the equilibrium rotation and radial electric field are found to be ruled by ripple [50]. So far, magnetic braking and turbulent stress were computed separately, ignoring any cross-talk. Based on Eq.2, the effect of turbulence on magnetic braking $\mathcal{M}$ is negligible as ripple wave numbers are non-resonant, hence hardly generated

via mode-coupling. On the other hand it appears that the turbulent Reynolds stress depends substantially on the ripple amplitude. This is shown on Fig.5c, which is obtained from three simulations performed with different ripple amplitudes. The residual stress is predicted to depend on the turbulent intensity shear and the $E \times B$ drift shear [32, 35] whilst turbulent viscosity depends only on the former. The residual stress can be expressed as:

$$\Pi_{res} = \sum_k k_\parallel k_\theta \left| \frac{e\phi_k}{T} \right|^2 \tau_k \qquad (6)$$

Where ϕ_k are the Fourier components of the electric potential, T the thermal energy, $k_\parallel$ and k_θ the parallel and poloidal wave number and τ_k a form factor [51]. The modification of the spectral intensity $|\phi_k|^2$ by ripple through mode-coupling in simulations is found negligible for large-scale modes. This implies that the turbulent viscosity is not affected by ripple. However the $E \times B$ shear modifies the parallel wave number by introducing radial asymmetry [34]. Ripple increases the radial electric field amplitude through neoclassical effects, so the E_r shear depends on the radial shape of the ripple amplitude. The model Π_{res} from Eq.6 comes from a mean field theory which holds when E_r is averaged over multiple turbulent structure lengths and correlation times, defining the coarse-grain average labelled $\langle . \rangle_{CG}$. This is done by time averaging over 10^5 cyclotron periods, i.e. about 50 correlation times, and performing a sliding radial average with a $50\rho_i$ window, i.e. about 5-6 correlation lengths. Mean E_r and associated shear are plotted in Fig.5a and 5b. The effect of ripple on these profiles is clear: both $\langle E_r \rangle_{CG}$ and $\langle E_r' \rangle_{CG}$ increase in amplitude with δ near the core region. The residual stress profile in Fig.5c is calculated as $\Pi_{res} = \Pi + \chi V_T'$ using the previously obtained viscosity. As the initial toroidal velocity in those simulation is zero, the viscous term is subdominant. It then appears that Π_{res} grows monotonically with δ and changes sign. $\langle E_r' \rangle_{CG}$ is correlated with the increase of $\langle \Pi_{res} \rangle_{CG}$ up to an offset, consistently with the numerical study [52]. The offset is likely explained by the impact of turbulent intensity shear and also by the effect of diamagnetism [35]. Finally, Fig.5d shows the averaged $-r^{-1}(r\Pi)'$ that appears in momentum conservation Eq.1. Regarding plasma rotation, positive/negative values of $\langle E_r'' \rangle_{CG}$ are found correlated with an increment of the toroidal velocity in the counter-/co-current direction due to turbulence. The critical ripple expression, derived without interplay, is still valid as the turbulent viscosity remains unchanged.

In summary, the effect of turbulent drive and magnetic braking has been studied on the same footing thanks to comprehensive gyrokinetic simulations. The critical ripple amplitude for which magnetic braking overcomes turbulence has been estimated theoretically and

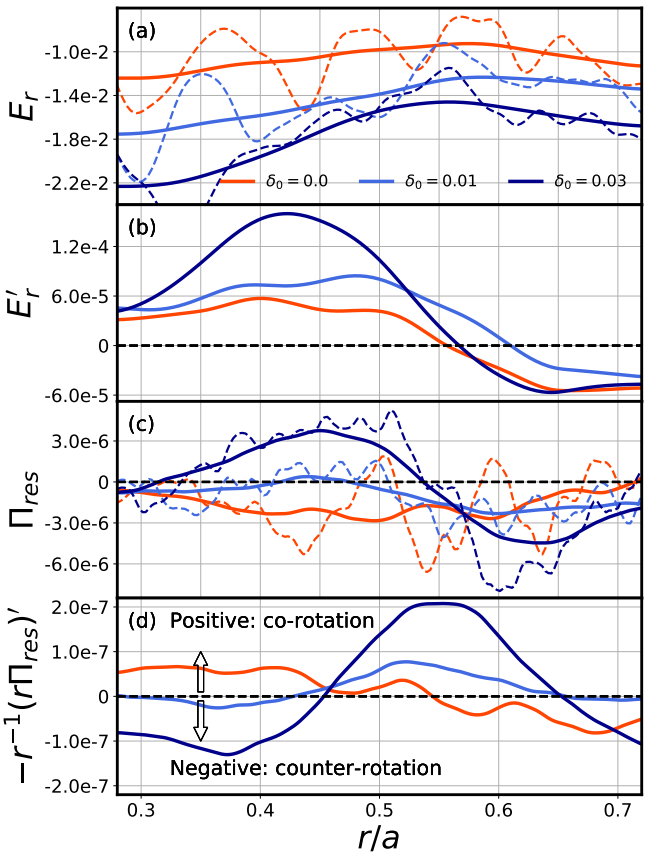

FIG. 5. Solid lines: radial profile of coarse-grained (temporally and spatially) radial electric field (a) and its shear (b), as well as residual stress (c) and the opposite of its divergence (d) for different ripple amplitudes. Dashed lines: time average only.

agrees with gyrokinetic simulations. An estimate for this threshold is proposed and its value in Tore Supra agrees with experimental measurements. Ripple also modifies the toroidal velocity by changing the turbulent Reynolds stress through the residual stress. In fact, the toroidal Reynolds stress is observed to vary monotonically with the ripple amplitude. It is observed in simulations that E_r' is enhanced in presence of ripple and that E_r' controls the residual stress. Robust knowledge of this intrinsic physics provides means to control the rotation. Indeed, recent work [53] demonstrated that restoring the magnetic symmetry is actually possible, giving some leverage on the magnetic braking strength.

The authors want to thank P. Diamond and C. Chen for helpful contributions. This work has been carried out within the framework of the EUROfusion Consortium, funded by the European Union via the Euratom Research and Training Programme (Grant Agreement No 101052200 — EUROfusion). Views and opinions expressed are however those of the author(s) only and do not necessarily reflect those of the European Union or

the European Commission. Neither the European Union nor the European Commission can be held responsible for them. This work was performed using HPC resources from GENCI, CCRT-TGCC and CINECA. This work was supported by funding from the European Union's Horizon 2020 research and innovation program under grant agreement no. 824158 (EoCoE II).

[1] P. Mantica *et al.*, Phys. Rev. Lett. **102**, 175002 (2009).
[2] P. C. de Vries *et al.*, Plasma Phys. Controlled Fusion **38**, 467–476 (1996).
[3] T. S. Hahm and K. H. Burrell, Phys. Plasmas **2**, 1648–1651 (1995).
[4] Y. Sakamoto *et al.*, Nucl. Fusion **41**, 865–872 (2001).
[5] M. F. F. Nave *et al.*, Phys. Rev. Lett. **105**, 105005 (2010).
[6] M. Rosenbluth and F. Hinton, Nucl. Fusion **36**, 55–67 (1996).
[7] A. Peeters *et al.*, Nucl. Fusion **51**, 094027 (2011).
[8] H. Urano *et al.*, Nucl. Fusion **47**, 706–713 (2007).
[9] W. Zhu *et al.*, Phys. Rev. Lett. **96**, 225002 (2006).
[10] J.-K. Park *et al.*, Phys. Plasmas **16**, 056115 (2009).
[11] Y. Sun *et al.*, Plasma Phys. Controlled Fusion **52**, 105007 (2010).
[12] A. J. Cole *et al.*, Phys. Plasmas **18**, 055711 (2011).
[13] C. Fenzi *et al.*, Nucl. Fusion **51**, 103038 (2011).
[14] X. Garbet *et al.*, Phys. Plasmas **17**, 072505 (2010).
[15] L. Kovrizhnykh, Nucl. Fusion **24**, 851–936 (1984).
[16] V. S. Tsypin *et al.*, Phys. Plasmas **5**, 3358–3365 (1998).
[17] K. C. Shaing, Phys. Fluids **26**, 3315 (1983).
[18] K. C. Shaing *et al.*, Phys. Fluids **27**, 1 (1984).
[19] K. C. Shaing *et al.*, Phys. Fluids **29**, 521 (1986).
[20] K. C. Shaing, Phys. Rev. Lett. **76**, 4364–4367 (1996).
[21] T. E. Stringer, Phys. Fluids **14**, 2177 (1971).
[22] J. Connor and R. Hastie, Nucl. Fusion **13**, 221–225 (1973).
[23] P. Yushmanov, Nucl. Fusion **22**, 315–324 (1982).
[24] P. Yushmanov, Nucl. Fusion **23**, 1599–1612 (1983).
[25] P. Yushmanov *et al.*, Nucl. Fusion **33**, 1293–1303 (1993).
[26] S. Matsuoka *et al.*, Phys. Plasmas **24**, 102522 (2017).
[27] S. Satake *et al.*, Comput. Phys. Comm. **181**, 1069 (2010).
[28] S. Satake *et al.*, Phys. Rev. Lett. **107**, 055001 (2011).
[29] N. C. Logan *et al.*, Phys. Plasmas **20**, 122507 (2013).
[30] K. Kim *et al.*, Nucl. Fusion **54**, 073014 (2014).
[31] P. Diamond *et al.*, Nucl. Fusion **49**, 045002 (2009).
[32] T. S. Hahm *et al.*, Phys. Plasmas **14**, 072302 (2007).
[33] A. G. Peeters *et al.*, Phys. Rev. Lett. **98**, 265003 (2007).
[34] Ö. D. Gürcan, P. Diamond, *et al.*, Phys. Plasmas **14**, 042306 (2007).
[35] Ö. D. Gürcan *et al.*, Phys. Rev. Lett. **100**, 135001 (2008).
[36] W. Solomon *et al.*, Nucl. Fusion **49**, 085005 (2009).
[37] F. J. Casson *et al.*, Phys. Plasmas **16**, 092303 (2009).
[38] M. Barnes *et al.*, Phys. Rev. Lett. **111**, 055005 (2013).
[39] Y. Camenen *et al.*, Phys. Rev. Lett. **102**, 125001 (2009).
[40] K. Ida and J. Rice, Nucl. Fusion **54**, 045001 (2014).
[41] Y. Idomura, Phys. Plasmas **21**, 022517 (2014).
[42] Y. Idomura, Phys. Plasmas **24**, 080701 (2017).
[43] R. E. Waltz *et al.*, Phys. Plasmas **18**, 042504 (2011).
[44] C.-C. Chen *et al.*, Phys. Plasmas **28**, 042301 (2021).
[45] P. W. Terry, Rev. Mod. Phys. **72**, 109–165 (2000).
[46] V. Grandgirard *et al.*, Comput. Phys. Commun. **207**, 35–68 (2016).
[47] See supplemental material at [link to be generated] for further details on the simulation parameters and justification of approximations, .
[48] L. Vermare *et al.*, Phys. Plasmas **18**, 012306 (2011).
[49] B. Chouli *et al.*, Plasma Phys. Controlled Fusion , 125007 (2015).
[50] E. Trier *et al.*, Nucl. Fusion **48**, 092001 (2008).
[51] X. Garbet *et al.*, Phys. Plasmas **9**, 3893–3905 (2002).
[52] W. X. Wang *et al.*, Phys. Rev. Lett. **102**, 035005 (2009).
[53] J.-K. Park *et al.*, Phys. Rev. Lett. **126**, 125001 (2021).
[54] P. N. Yushmanov, Reviews of plasma physics, edited by B. B. Kadomtsev (Consultants Bureau, New York) (1991).